

# Characterizing and controlling the inherent dynamics of cyclophilin-A

Jennifer Schlegel,<sup>1</sup> Geoffrey S. Armstrong,<sup>2</sup> Jasmina S. Redzic,<sup>1</sup> Fengli Zhang,<sup>3</sup> and Elan Zohar Eisenmesser<sup>1\*</sup>

<sup>1</sup>Department of Biochemistry and Molecular Genetics, School of Medicine, University of Colorado Denver, Aurora, Colorado 80045

<sup>2</sup>Department of Chemistry and Biochemistry, University of Colorado at Boulder, Boulder, Colorado 80309

<sup>3</sup>National High Magnetic Field Laboratory, Tallahassee, Florida 32310

Received 23 September 2008; Revised 15 January 2009; Accepted 17 January 2009

DOI: 10.1002/pro.89

Published online 12 February 2009 proteinscience.org

**Abstract:** With the recent advances in NMR relaxation techniques, protein motions on functionally important timescales can be studied at atomic resolution. Here, we have used NMR-based relaxation experiments at several temperatures and both 600 and 900 MHz to characterize the inherent dynamics of the enzyme cyclophilin-A (CypA). We have discovered multiple chemical exchange processes within the enzyme that form a “dynamic continuum” that spans 20–30 Å comprising active site residues and residues proximal to the active site. By combining mutagenesis with these NMR relaxation techniques, a simple method of counting the dynamically sampled conformations has been developed. Surprisingly, a combination of point mutations has allowed for the specific regulation of many of the exchange processes that occur within CypA, suggesting that the dynamics of an enzyme may be engineered.

**Keywords:** chemical exchange; cyclophilin-A; dynamics; peptidyl-prolyl isomerase; relaxation; nuclear magnetic resonances; enzymes; NMR spectroscopy

## Introduction

Although our understanding of protein sequence and structure has grown exponentially within the last 20 years, the role of dynamics in protein function has only recently begun to be studied at atomic resolution. Advancements in NMR relaxation experiments that probe protein motions on the micro-millisecond ( $\mu$ s-ms) timescale have allowed us to begin studying a

diverse array of dynamic functions that include disulfide isomerization,<sup>1</sup> protein folding,<sup>2–5</sup> metal binding,<sup>6</sup> and the dynamics associated with enzyme conformational changes.<sup>7–9</sup> Enzymes are at the forefront of understanding the relationship between protein dynamics, sequence, structure, and function, since they are dependent on  $\mu$ s-ms conformational changes for catalysis. New innovative approaches that utilize these recent experimental techniques will allow us to go beyond the static structural descriptions of enzymes to help understand how dynamics have been evolutionarily selected for function.

Motions on the  $\mu$ s-ms timescale have been detected both in the presence and absence of substrates within many of the enzymes studied to date, implying that inherent flexibility is important for function.<sup>10</sup> Although the details of these motions are altered by the substrates, they localize to similar regions, and are on similar timescales as catalysis. For example, both free RNaseA<sup>11–13</sup> and free cyclophilin-A (CypA)<sup>8,14</sup> exhibit conformational exchange rates on the order of 1000–3000 s<sup>-1</sup> that are similar to their rates of turnover. Such similar rates may

---

Additional Supporting Information may be found in the online version of this article.

*Abbreviations:* CPMG, Carr-Purcell-Meiboom-Gill; CypA, cyclophilin-A; HMQC, heteronuclear-multi-quantum-coherence; HSQC, heteronuclear-single quantum coherence;  $k_{ex}$ , chemical exchange rate; NMR, nuclear magnetic resonance;  $R_2$ , transverse relaxation rate.

Grant sponsor: NSF; Grant number: MCB-0820567.

\*Correspondence to: Elan Zohar Eisenmesser, Department of Biochemistry and Molecular Genetics, School of Medicine, University of Colorado Health Sciences Center, Aurora, CO 80045. E-mail: Elan.Eisenmesser@UCDenver.edu

also suggest that conformational rearrangements in the free enzymes are similar to those during catalysis, yet this has not been directly shown. For CypA that is the enzyme under study here, a clear understanding as to how these inherent movements may be correlated and how they compare with catalysis remains unclear.

CypA catalyzes the reversible isomerization of peptidyl-prolyl bonds (i.e. cis/trans isomerization) and plays multiple biological roles that include protein folding and signal transduction.<sup>15</sup> CypA is also involved in multiple diseases including cancer, inflammatory disorders, and viral infections.<sup>16,17</sup> Thus, there has been great interest in designing inhibitors to block the detrimental roles of CypA during disease progression<sup>18,19</sup> and an understanding of its dynamic behavior may augment rational based approaches. Here, we have used mutagenesis together with several NMR methods aimed at probing protein motions at both multiple temperatures and multiple static field strengths to characterize the inherent dynamics of CypA.

We have discovered that much more of CypA undergoes exchange than previously thought<sup>8,14</sup> and that multiple exchange processes occur within the enzyme that form a “dynamic continuum” at higher temperatures. These exchange events range from relatively fast motions on one side of the protein to much slower motions on the other side and the associated exchange rates vary by approximately six-fold. Through mutagenesis we have developed a methodology that has allowed us to “count” the number of dynamically sampled conformations for many residues and specifically control the dynamics of an entire region of CypA. Our studies suggest that much of CypA undergoes a dominant two-site exchange. To our knowledge, this is the first report that has employed mutagenesis to selectively control the dynamics of a protein by combining point mutations in a rational-based manner. Such findings may have powerful implications in the future engineering of enzymes with both dynamic and functional attributes.

## Results

### **Combining higher static field strengths, lower temperatures, and deuteration, reveal that nearly half of CypA undergoes chemical exchange**

$R_2$  relaxation rate constants have been used extensively to monitor the  $\mu\text{s}$ - $\text{ms}$  motions of many proteins, however, a major bottleneck in characterizing the majority of these motions within a given protein is the sensitivity of such measurements. This sensitivity issue is exemplified by Eq. (1) that describes a simple two-site model of fast exchange on the chemical shift time-scale ( $k_{\text{ex}} > \Delta\omega$ ), such that  $A \xrightleftharpoons[k_A]{k_B} B$ . Here,  $P_A$  and  $P_B$  represent the major and minor sampled populations, respectively,  $\Delta\omega$  is the chemical shift differences between the states (i.e.  $\Delta\omega_N$  for  $^{15}\text{N}$  and  $\Delta\omega_H$  for  $^1\text{H}$ ,

etc.),  $k_{\text{ex}}$  is the kinetic rate of exchange that is the sum of  $k_A$  and  $k_B$  (i.e.  $k_{\text{ex}} = k_A + k_B$ ), and  $R_2^\circ$  is the transverse relaxation rate in the absence of exchange. Chemical exchange is defined as  $R_{\text{ex}}$  and is simply  $R_2 - R_2^\circ$ . If either the minor sampled population or the chemical shift difference is too small then there will be a negligible contribution to  $R_{\text{ex}}$  despite the physical existence of motions. The advent of Carr–Purcell–Meiboom–Gill (CPMG)  $R_2$  relaxation dispersion experiments have allowed for an increased sensitivity to chemical exchange compared to classical  $R_2$  measurements. Here, a variable refocusing field is applied as opposed to classical  $R_2$  measurements that impart only a single refocusing field. The contribution of exchange, and therefore  $R_2$ , is modulated by this applied CPMG field (i.e.  $\nu_{\text{cpmg}}$ ), resulting in an effective transverse rate called  $R_2^{\text{eff}}$  that is fit to a modified version of Eq. (1), called the Carver–Richards equation.<sup>20–22</sup>  $R_2$ -CPMG experiments have proven invaluable in monitoring motions at atomic resolution since the fit dispersion data provides not only the identification of motions, but also the biophysical parameters that govern such motions.

$$R_2 = R_2^\circ + R_{\text{ex}}; R_{\text{ex}} = P_A P_B \frac{\Delta\omega^2}{k_{\text{ex}}} \quad (1)$$

For free CypA, previous  $R_2$ -CPMG experiments performed at 600 MHz and  $10^\circ\text{C}$  identified less than 30 residues undergoing chemical exchange.<sup>8,14</sup> However, the quality of data for many of these residues made it difficult to reliably characterize their motions. Thus, we have now combined deuteration with the highest field strength currently commercially available, 900 MHz, to more thoroughly probe the inherent dynamics of CypA. Deuteration increases the sensitivity of chemical exchange by in part lowering the apparent  $R_2^\circ$  and higher field strengths allow for the detection of residues exhibiting very small chemical shift changes to be identified as shown by the quadratic field dependence in Eq. (1).

Using  $^{15}\text{N}$ - $R_2$ -CPMG relaxation dispersion measurements on  $^2\text{H}$ ,  $^{15}\text{N}$ -CypA (referred to as  $R_2$ -CPMG for the simplicity), 75 amides that represent nearly half of the residues within CypA give rise to measurable exchange over  $0.5 \text{ s}^{-1}$  at 900 MHz and  $0^\circ\text{C}$  [Fig. 1(A), Supporting Information Table S1]. This is in comparison with the 48 residues at  $10^\circ\text{C}$  and 40 residues at  $20^\circ\text{C}$  that are all considerably more than the number detected previously at  $10^\circ\text{C}$  and 600 MHz using  $^{15}\text{N}$ -labeling alone.<sup>8</sup> The vast majority of residues exhibiting chemical exchange are relegated to the active site and include the catalytic residue R55. On the basis of the co-crystal structure complexes, the guanidino side chain of R55 has previously been proposed to weaken the double-bond character of prolyl-peptide bonds<sup>24,25</sup> and in accord with this, we have previously shown that R55 exhibits chemical exchange

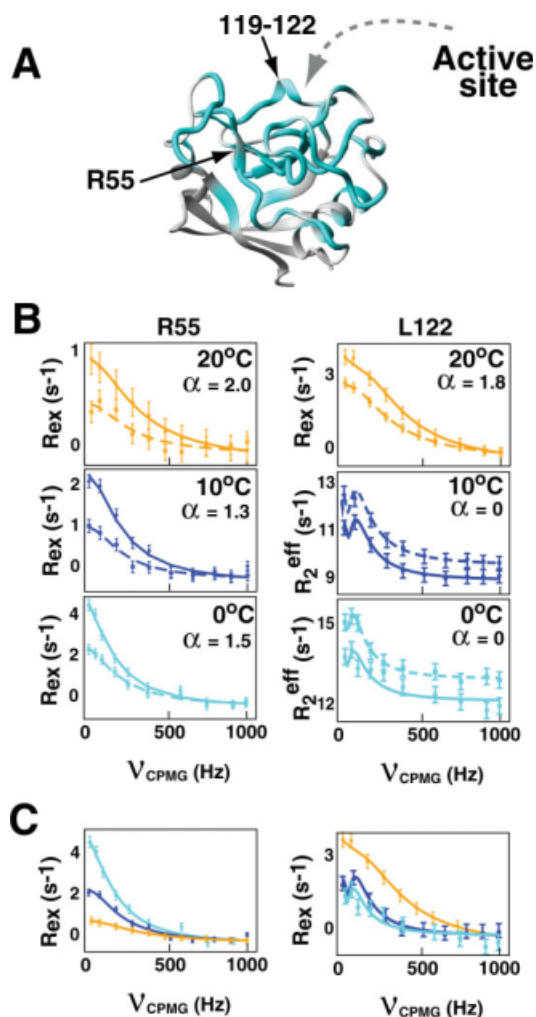


**Figure 1.** Free CypA undergoes exchange on multiple chemical shift timescales. **(A)** Nearly half of CypA exhibits chemical exchange contributions (cyan) above  $0.5 \text{ s}^{-1}$  (Supporting Information Table S1). **(B)** The static magnetic field dependence of chemical exchange is used to calculate  $\alpha$  at  $20^\circ\text{C}$ ,  $10^\circ\text{C}$  and  $0^\circ\text{C}$  from Supporting Information Table S2.<sup>23</sup> R2-CPMG dispersion is shown at 600 MHz (dashed lines, ■) and 900 MHz (straight lines, ●) for R55 and L122. Dispersion curves for L122 at  $10^\circ\text{C}$  and  $0^\circ\text{C}$  exhibit no static field dependence (i.e.  $\alpha = 0$ ) and thus, the absolute  $R_2^{\text{eff}}$  is shown for clarity to avoid overlap of their calculated fits. **(C)** The temperature dependence of  $R_{\text{ex}}$  is shown for these same residues and is in good agreement with the static magnetic field dependence.  $R_{\text{ex}}$  increases with lower temperatures for R55 and decreases for L122, indicating fast exchange and slow exchange, respectively.<sup>1</sup> Data were collected at  $20^\circ\text{C}$  (orange),  $10^\circ\text{C}$  (blue), and  $0^\circ\text{C}$  (cyan). [Color figure can be viewed in the online issue, which is available at [www.interscience.wiley.com](http://www.interscience.wiley.com).]

during catalysis of a model peptide substrate.<sup>8,14</sup> However, this is the first report to directly measure the exchange of this residue in the free wild-type enzyme and directly show that its exchange rate is similar to the catalytic rate during turnover (see below).

### The chemical shift timescales of CypA exchange as probed by both the static field dependence and temperature dependence of R2-CPMG dispersion

Identifying the timescale of chemical exchange for each residue of a macromolecule is critical for several reasons. First, in the limit of very slow exchange R2-CPMG dispersion data are poorly described by the Carver–Richards equation, requiring the use of a “slow exchange equation” described later for some of these exchanging residues.<sup>3</sup> Thus, it is important to know the chemical shift timescale to apply the correct analysis to R2-CPMG dispersion data. Second, while a single dynamic process can include residues that exchange on multiple chemical shift timescales, identifying these timescales may provide insight as to the explicit structural changes involved. For example, large chemical shifts may suggest that the structural changes involve aromatic residues.

There are several methods that can probe the chemical shift timescale of exchange. Palmer and co-workers have shown that the timescale of exchange can be measured as a function of the static magnetic field and can be quantitatively described by the parameter called alpha (i.e. the  $\alpha$ -factor).<sup>23</sup> This parameter is defined as  $\alpha = \frac{(B_{02}+B_{01})}{(B_{02}-B_{01})} * \frac{(R_{\text{ex}2}-R_{\text{ex}1})}{(R_{\text{ex}2}+R_{\text{ex}1})}$  where  $B_{02}$  and  $B_{01}$  represent the static magnetic fields, 600 and 900 MHz, respectively, used in this study, and  $R_{\text{ex}}$  the associated exchange contributions at each field. In the limit of slow exchange, there is no dependence on field strength for the chemical exchange contribution and  $\alpha$  is between 0 and 1. In the limit of fast exchange, there is a quadratic dependence on the static field for the exchange contribution and  $\alpha$  is between 1 and 2. The temperature dependence of chemical exchange can also be used to define the chemical shift timescale.<sup>1</sup> Specifically, the temperature dependence is completely opposite for the case of slow exchange versus that of fast exchange, with the maximum contribution at intermediate exchange (i.e. coalescence,  $k_{\text{ex}} = \Delta\omega$  for a system undergoing a two-site exchange). Thus, both the static field dependence and temperature have been used to define the timescale of chemical exchange exhibited by residues within CypA.

A comparison of R2-CPMG dispersion between 600 and 900 MHz reveals that CypA undergoes exchange on multiple chemical shift timescales, which is in contrast to previous investigations that had assumed all residues undergo fast exchange.<sup>8,14</sup> The calculated  $\alpha$ -factors are shown in Supporting Information Table S2 for those residues that exhibit measurable exchange at both static field strengths and examples are shown for R55 and L122 [Fig. 1(B)]. Most residues, such as the catalytic residue R55, exhibit intermediate-fast exchange at all temperatures [Fig. 1(B), left]. In contrast, residues within the 3,10- $\alpha$ -helix (i.e. residues 119–122) and several neighboring residues to this helix (K91, H92, H126, and V128) exchange on

the intermediate-slow timescale of chemical exchange at 20°C and are at the slow-exchange limit at 10°C and 0°C. Such slow exchange is immediately apparent in the sinusoidal behavior of their exchange contributions at the lower  $\nu_{\text{cpmg}}$  fields imparted [e.g., L122 at 0°C in Fig. 1(B), right]. These static magnetic field comparisons are in good agreement with the temperature dependence of these residues, as shown for R55 and L122 [Fig. 1(C)]. Here, exchange decreases with decreasing temperature for L122 and increases with decreasing temperature for R55 as predicted for residues undergoing slow and fast exchange, respectively.<sup>1</sup> Interestingly, several sequential residues exhibit exchange on different timescales and this may suggest that the exchange events monitored are associated with very localized structural changes. For example, sequential residues that comprise the  $\beta$ -sheet within the core of the enzyme, such as residues 55,56 and 62,63, exchange on multiple timescales at both 20°C and 10°C (Supporting Information Table S2). Interestingly, from 10°C to 0°C several of these core residues exhibit a transition from slow to fast exchange on the chemical shift timescale that may seem counterintuitive at first. However, the actual exchange rates themselves do not increase at the lower temperatures, but simply the exchange rates relative to the chemical shift differences in sampled states increase (i.e.  $k_{\text{ex}} > \Delta\omega$ ). Thus, the absolute value of  $\Delta\omega$  decreases at 0°C for several chemical exchange events and may suggest that some of the associated conformational changes have been “frozen out.” For example, several of the 22 aromatic residues that are concentrated within the core of CypA may exhibit a reduction in ring flipping at 0°C.

It is important to note that in this limit of very slow exchange, the R2-CPMG dispersion profile becomes completely dependent on only the forward rate constant,  $k_A$ , in a simple two-site exchange. For slowly exchanging residues such as residues 119–122 described earlier, the accuracy of the Carver–Richards equations are gravely reduced and a “slow exchange equation” may be applied as previously described<sup>3</sup> and shown in Eq. (2). Here,  $R_{2A}$  is the transverse relaxation rate of the nucleus in site A without chemical exchange and the remaining parameters are as already described. However, caution must be taken in applying this equation since it is ONLY valid when the individual microscopic rate constants are slower than the imparted rate of pulsing (i.e.  $k_A, k_B < 1/\tau_{\text{cpmg}}$ , where  $\tau_{\text{cpmg}}$  is the spacing between 180° refocusing pulses,  $1/\tau_{\text{cpmg}} = 4^* \nu_{\text{cpmg}}$  and  $k_{\text{ex}} = k_A + k_B$  for a two-site exchange as described earlier). The largest  $\tau_{\text{cpmg}}$  value used at 10°C and 0°C was 7.5 ms and this means that both  $k_A$  and  $k_B$  must be less than  $133 \text{ s}^{-1}$  ( $= 1/7.5 \text{ ms}$ ). Although this is most certainly the case for the smaller microscopic rate constant  $k_A$ , the value of  $k_B$  is unknown and could potentially approach or even exceed the pulsing rate. However, since application of

the full Carver–Richards equation for such slowly exchanging residues (on the chemical shift timescale) leads to uncertainties for  $k_{\text{ex}}$  that are larger than the values themselves, Eq. (2) is used as an approximation for the forward rate constant,  $k_A$ . Finally, it is important to note that at the limit of slow exchange for which residues such as 119–122 safely lies within (i.e. there is no static field dependence and  $\alpha = 0$ ), the exchange contribution itself,  $R_{\text{ex}}$ , is similar to  $k_A$ . Thus, the amplitudes of these dispersion profiles for slowly exchanging residues already define a range for this forward rate constant (i.e.  $\sim 1\text{--}2 \text{ s}^{-1}$  for residues such as 119–122).

$$R2^{\text{eff}} = R2^A + k_A - k_A \frac{\sin(\Delta\omega/4\nu_{\text{CPMG}})}{\Delta\omega/4\nu_{\text{CPMG}}} \quad (2)$$

### **Multiple dynamic processes occur within CypA at a single temperature and many of the exchange processes exhibit different temperature dependencies**

Although earlier we have shown that residues within free CypA exhibit a wide range in chemical exchange on the chemical shift timescale (i.e.  $k_{\text{ex}}$  relative to  $\Delta\omega$ ,  $k_{\text{ex}}/\Delta\omega$ , varies for each residue), here we show that residues within free CypA also exhibit a wide range in the absolute exchange rates themselves. Using R2-CPMG dispersion measured at both 600 and 900 MHz, amide dispersion curves were independently calculated for each residue. The use of two static field strengths increases the accuracy of calculated parameters derived from R2-CPMG dramatically, with additional fields shown to have much less of an effect.<sup>26</sup> At 20°C, residues within free CypA exhibit approximately a six-fold difference in their extracted exchange rates, ranging from a calculated  $\sim 6000 \text{ s}^{-1}$  on one side of CypA to  $\sim 1000 \text{ s}^{-1}$  on the opposite side of the enzyme [Fig. 2(A)]. Such different exchange processes are immediately apparent in the fit dispersion curves themselves [Fig. 2(B)] and appear to form a “dynamic continuum” at this temperature. For example, at 20°C, exchange is so fast for most residues comprising the loop region of residues 65–84 and neighboring residues 110–111 that the R2-CPMG dispersion curves are linear. In contrast, residues 119–122 that comprise a short 3,10-helix and several residues that lay immediately adjacent to this region (K91, H92, H126, and V128) exhibit much slower exchange. For this region the exchange contributions are essentially suppressed at the highest refocusing field applied ( $\nu_{\text{CPMG}} = 1000 \text{ Hz}$ ).

CypA residues undergoing different exchange rates at 20°C also exhibit different temperature dependencies, confirming that the enzyme undergoes multiple exchange processes on the  $\mu\text{s}$ –ms timescale (Fig. 3 and Table I). R2-CPMG dispersion collected at three temperatures (0, 10, and 20°C) and two static magnetic

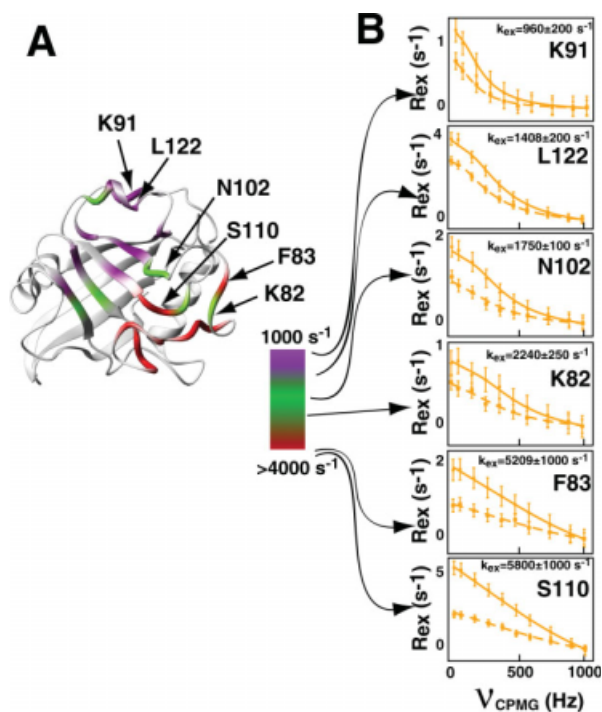


**Figure 2.** The chemical exchange of CypA represents a dynamic continuum. **(A)** R2-CPMG derived chemical exchange rates,  $k_{ex}$ , are shown on a continuous scale from purple-to-green-to-red representing an increase from 1000  $s^{-1}$  (purple) to nearly 6000  $s^{-1}$  (red) at 20°C. **(B)** R2-CPMG dispersions are shown at both 600 MHz (dashed line, ■) and 900 MHz (straight line, ●) for several residues within CypA demonstrating a dynamic continuum at 20°C. [Color figure can be viewed in the online issue, which is available at [www.interscience.wiley.com](http://www.interscience.wiley.com).]

fields (600 and 900 MHz) reveal that many of the core residues of CypA exhibit the least temperature dependence. These core residues primarily comprise  $\beta$ -strands at the bottom of the active site such as W113 [Fig. 3(B), middle panels]. In contrast, both the faster and slower exchanging residues at 20°C described earlier do slow down considerably with temperature as exemplified by I78 and T119, respectively [Fig. 3(B), left and right panels].

Several important cautionary notes must be addressed for these individual extracted exchange rates (Table I). First, we have applied a simple two-site exchange model to describe the measured R2-CPMG dispersion. Without the preexisting knowledge of a more complicated process there is no apparent reason to employ a more complicated model such as a three-site exchange. However, later we have sought innovative ways to combine mutagenesis with NMR relaxation measurements to specifically identify how many conformations are explored by the chemical exchange events measured here. Here, we report the total exchange rate (i.e.  $k_{ex}$ ), since the model selection does not drastically affect this value but only the individual microscopic rate constants. Second, for slowly exchanging residues such as residues 119–122, only

the forward rate constant (i.e.  $k_A$ ) can be extracted using the slow-exchange equation at both 0 and 10°C, and this is what is listed in Table I. Third, the individual microscopic rate constants, their associated populations, and the chemical shifts are poorly defined on a per residue basis for residues undergoing fast exchange. Globally fitting residues has been shown to decrease such uncertainties for these parameters, yet, there is no apparent rationale for globally fitting residues within CypA and it is unclear as to which residues should be included in such global fits. In fact, several neighboring residues immediately adjacent to one another, such as S110 and N102 at 20°C (see Fig. 2), exhibit very different exchange rates that argue against completely cooperative exchange within particular regions of CypA.

### Counting conformations and probing the dynamic network of CypA using dynamics-based mutagenesis

If dynamic fluctuations within enzymes have been evolutionarily selected for their catalytic function, then cyclophilins may sample two dominant conformations

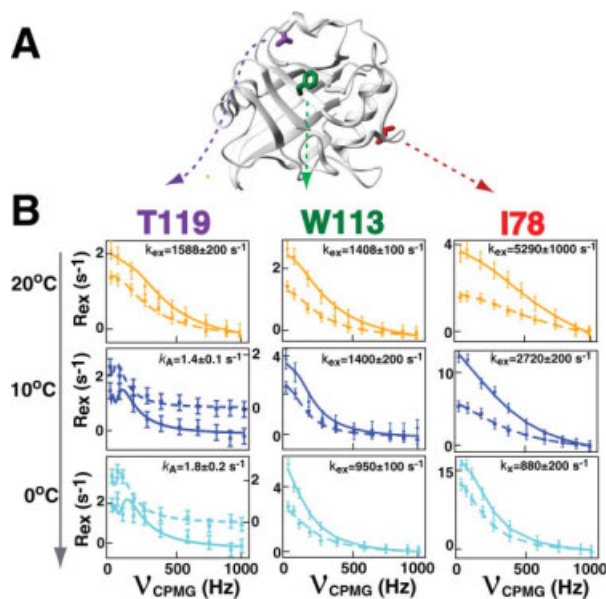


**Figure 3.** Several chemical exchange processes occur within free CypA. **(A)** The positions of three residues within CypA that exhibit different temperature dependencies are shown and include T119 (magenta), W113 (green), and I78 (red). **(B)** The R2-CPMG dispersion profiles are shown for these same residues at 20°C (orange), 10°C (dark blue), and 0°C (light blue) at both 600 MHz (dashed line, ■) and 900 MHz (straight line, ●). The extracted exchange rates,  $k_{ex}$ , are shown for each simultaneous fit of the data at both static magnetic fields. For T119 the axis for each field at 0°C and 10°C are offset for 600 MHz (right axis) for clarity since there is no static magnetic field dependence for this residue at these temperatures and their exchange is difficult to see when superimposed. [Color figure can be viewed in the online issue, which is available at [www.interscience.wiley.com](http://www.interscience.wiley.com).]

**Table I.** Amide Chemical Exchange Rates of CypA. Chemical Exchange Rates,  $k_{ex}$ , were Calculated on a per Residue Basis Using Both 600 MHz and 900 MHz R2-CPMG Dispersion. Exchange Rates are not Reported for Those Residues Exhibiting Uncertainties Greater Than the Calculated Rates or for Those Residues Exhibiting Exchange  $<0.5\text{ s}^{-1}$  at the Given Temperature

Residue	0°C	10°C	20°C
48	1456 ± 370		
55	1159 ± 150	1176 ± 200	1584 ± 340
56	1070 ± 160		1239 ± 400
57	1511 ± 360		
61			1354 ± 350
62	1534 ± 180	1542 ± 300	
63	1456 ± 340	2417 ± 460	1957 ± 310
65	811 ± 200	2129 ± 400	5114 ± 1000
66	559 ± 180	2849 ± 230	5452 ± 1000
67	189 ± 260	3628 ± 450	4193 ± 1000
68	934 ± 350		
69	725 ± 400		
72		1200 ± 300	5794 ± 2800
73			
74		3666 ± 350	
75	748 ± 170		
76	956 ± 100	2578 ± 120	5326 ± 1000
77	562 ± 150	2558 ± 160	5490 ± 1000
82	1070 ± 120	O.L.	2240 ± 250
83	633 ± 100	2610 ± 280	5201 ± 1000
84	1200 ± 400		
91	$k_A = 0.54 \pm 0.07^a$	$k_A = 0.85 \pm 0.18^a$	960 ± 200
92	$k_A = 1.64 \pm 0.15^a$	$k_A = 2.15 \pm 0.11^a$	1072 ± 200
96	$k_A = 1.01 \pm 0.11^a$	$k_A = 0.9 \pm 0.15^a$	1351 ± 250
98	1159 ± 200	2130 ± 400	1031 ± 300
99	460 ± 100	400 ± 100	1320 ± 100
102	1511 ± 150	1524 ± 400	1750 ± 100
109	1269 ± 150	3041 ± 1000	1700 ± 600
110	684 ± 120	3142 ± 500	5800 ± 1000
111	1008 ± 100	2737 ± 200	4864 ± 1500
113	950 ± 100	1400 ± 200	1400 ± 100
119	$k_A = 1.84 \pm 0.14^a$	$k_A = 1.41 \pm 0.08^a$	1588 ± 200
120	$k_A = 1.85 \pm 0.12^a$	$k_A = 2.74 \pm 0.13^a$	1366 ± 100
122	$k_A = 1.84 \pm 0.11^a$	$k_A = 2.33 \pm 0.13^a$	1408 ± 200
126			1453 ± 160
128			1038 ± 240

<sup>a</sup> Only the forward rate constant,  $k_A$ , could be extracted due to slow exchange (see text). Both  $k_A$  and the respective uncertainties were calculated using the “slow exchange equation” described in Materials and Methods.

in the absence of substrates just as they do during peptidyl-prolyl *cis/trans* isomerization of substrates. Free cyclophilins would then undergo dynamic fluctuations that sample two dominant conformations similar to their bound conformations of catalyzed substrates. In other words, if inherent motions within CypA correspond to the physical conformations that occur during turnover, then “*cis-like*” and “*trans-like*” conformations may be sampled for each residue even prior to catalysis. Here, we have begun characterizing the dynamic exchange processes identified earlier by using an approach that combines mutagenesis with relaxation experiments. The primary question that we have sought to address is whether the inherent dynamics of CypA have been explicitly preprogrammed for sampling two conformations or a more complicated exchange process? Such a finding would also validate the use of a simple two-site model that could be an oversimplification for many dynamic processes.

Mutagenesis is an obvious yet, powerful way to probe protein motions and here we have built on our previous discovery that has shown enzyme dynamics may be altered by the introduction of point mutations.<sup>8</sup> Specifically, two point mutations within CypA, R55A (producing CypA<sup>R55A</sup>), and K82A (producing CypA<sup>K82A</sup>), were previously found to either decrease or increase the dynamic sampling of a minor population for many residues throughout the enzyme, respectively. R55 is the catalytic residue and K82 is on a loop adjacent to the active site that has not been found to make any direct contact with substrates. The dynamic effects of these mutations were found to impart measurable changes to R2-CPMG dispersion profiles for residues nearly 20 Å away. Such distal changes could not be explained by local effects ( $\Delta\omega$ ), but rather indicated that these mutations impart global effects to chemical exchange ( $P_A$ ,  $P_B$ , and  $k_{ex}$ ). Furthermore, each of these mutations was found to

produce similar effects on R2-CPMG dispersions for multiple residues of CypA, either decreasing the amplitudes within R2-CPMG dispersion profiles for many residues within CypA<sup>R55A</sup> or increasing such amplitudes for the same residues within CypA<sup>K82A</sup>. Since mutagenic changes solely to  $\Delta\omega$  would be expected to be somewhat random, this too suggested that changes were incurred to other phenomena that dictated chemical exchange beyond the local chemical environments. The extracted  $k_{\text{ex}}$  values for these R2-CPMG dispersions were nearly the same for each residue as their wild-type counterpart, and thus, global changes in R2-CPMG amplitudes could only be due to changes in the minor population for each residue ( $P_{\text{B}}$ ). While this was further confirmed by alternative measures of these populations using HSQC/HMQC experiments described later, only a subset of residues could previously be measured.<sup>8</sup> Thus, here we have analyzed both of these mutants at higher fields, multiple temperatures and, importantly, we have extended these prior studies to include the double mutation CypA<sup>R55A,K82A</sup>, which has further contributed to our understanding of these dynamic exchange processes.

The rationale for this double mutation, CypA<sup>R55A,K82A</sup>, is critical for these studies and is therefore described in the following. For a system undergoing a dominant two-site exchange, the sampling of a minor population can only be decreased or increased. Thus, when the populations are skewed, as is the case for CypA (i.e.  $P_{\text{A}} \gg P_{\text{B}}$ ),<sup>8</sup> a combination of single mutations that each independently either decreases or increases a dynamically sampled minor population (i.e.  $P_{\text{B}}$ ) is expected to be a linear combination of both. This can be directly measured as a contribution to  $R_{\text{ex}}$  using R2-CPMG experiments (i.e. amplitude changes). A secondary independent measure of this can also be detected as a chemical shift difference ( $\Omega$ ) between heteronuclear-single quantum coherence (HSQC) and heteronuclear-multi-quantum coherence (HMQC) spectra, referred to herein as H(S/M)QC experiments and further described later. Thus, we have attempted to combine individual point mutations to regulate CypA motions.

CypA residues can broadly be divided into three regions based on their dynamic responses to the individual point mutations, CypA<sup>R55A</sup> and CypA<sup>K82A</sup>, and the double mutation CypA<sup>R55A,K82A</sup> and described herein as regions I, II, and III. Region I exhibits dynamic properties within CypA<sup>R55A,K82A</sup> that are a linear combination of the individual point mutations while regions II and III do not exhibit such a linear dependence but still differ from each other. The majority of amide resonances within all mutants differ from wild-type CypA by less than 0.1 ppm as monitored by <sup>15</sup>N-HSQC spectra, indicating the intact global fold remains and large structural changes have not been induced. Only three amides that exhibit chemical exchange are in close proximity to either the mutated side chain of R55 (specifically, I56 and Q63) or K82

(specifically, Y83), yet even these residues exhibit mutagenic-induced changes to their exchange that is consistent with their neighboring residues suggesting once again that their corresponding amide  $\Delta\omega$  values were not significantly altered by these mutations. Importantly, the fact that all residues within each region described below exhibit the same mutagenic response implies that the imparted changes are not simply local environmental changes (i.e. chemical shift changes of either sampled state,  $\omega_{\text{A}}$  and  $\omega_{\text{B}}$ ), which would be expected to result in a distribution of altered exchange contributions due to altered  $\Delta\omega$  values. Instead, these mutations must result in dynamic changes to the two remaining variables in Eq. (1) that are either the sampled populations or exchange rates. As the exchange rates are nearly identical for all mutants then the mutagenic changes in chemical exchange are primarily due to their effects on populations. Thus, although we will begin to discuss the changes to chemical exchange as amplitudes in regard to the actual data, the underlying physical changes are due to populations and this is further discussed below. Residues that exhibit a linear response in chemical exchange to mutations (i.e. region I) will be discussed separately from those that do not (i.e. regions II and III).

**Residues in which chemical exchange within CypA<sup>R55A,K82A</sup> is a linear combination of that within CypA<sup>R55A</sup> and CypA<sup>K82A</sup> (region I)**

Approximately half of the residues with detectable dispersion within the wild-type CypA exhibit an additive effect to  $R_{\text{ex}}$  from both of the single mutations within CypA<sup>R55A,K82A</sup>, as would be predicted for a simple two-site dynamic exchange process [Fig. 4(A) and Supporting Information Table S3]. Thus, the dynamic exchange that was altered by one mutation has been compensated by the other mutation, resulting in a double mutant that exhibits near wild-type dynamic properties for this large subset of residues. This region (i.e. region I) includes the loop region adjacent to the active site of residues 65–84, the neighboring loop of residues 110–111, and residues within 29–46 that comprise  $\alpha$ -helix-1 [Fig. 4(B)]. The exchange of residues 29–44 can only be detected at 0°C that is likely due to small chemical shift differences between sampled states (i.e.,  $\Delta\omega$ ). Conversely, several amides within the loop region of residues 65–84 that lay immediately adjacent to the active site are severely linebroadened at 900 MHz, which suggests that these residues exhibit large chemical shift differences between sampled states. As quantifying intensities from severely linebroadened resonances results in large uncertainties for R2-CPMG dispersion analysis,<sup>26</sup> our lower field data at 600 MHz provides a more accurate assessment of dispersion for these residues [Fig. 4(A)]. Finally, this striking example of controlling the exchange contributions for multiple residues (i.e.,  $R_{\text{ex}}$ ) by mutagenesis in a specific and measurable manner once again suggests

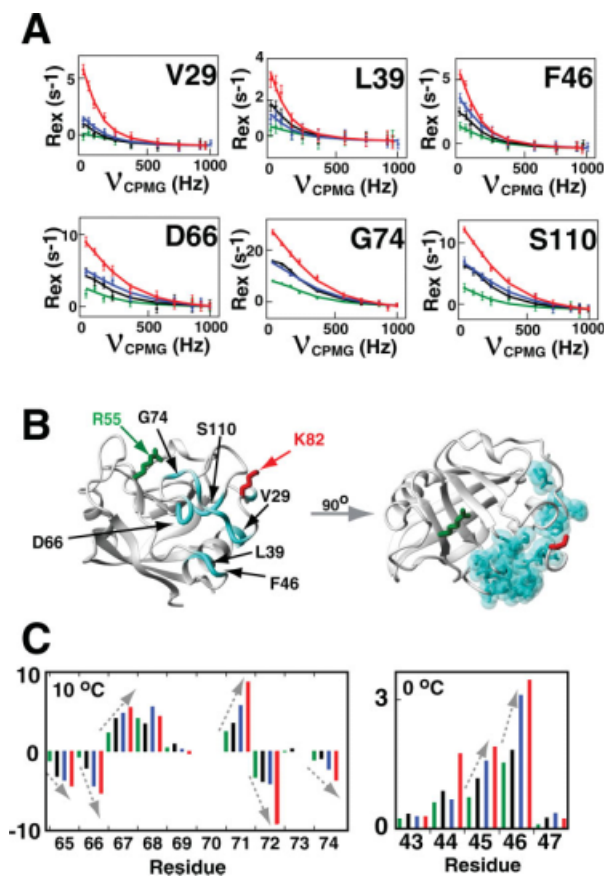


**Figure 4.** The chemical exchange of many residues within CypA exhibit a linear combination of individual point mutations (described as region I). **(A)** R2-CPMG dispersion profiles are shown for residues within CypA<sup>R55A</sup> (green), CypA<sup>R55A,K82A</sup> (black), wild-type CypA (blue), and CypA<sup>K82A</sup> (red). The amplitudes of R2-CPMG dispersion are a linear combination of each individual mutation for many residues, suggesting the minor sampled population for each exchange can be selectively altered as described by Eq. (1). Calculated lines were independently fit for V29, L39, and F46 at 900 MHz measured on <sup>2</sup>H<sup>15</sup>N-labeled proteins at 0 °C and for D66, G74, and S110 at 600 MHz for <sup>15</sup>N-labeled proteins measured at 0 °C. **(B)** All residues exhibiting this similar mutagenic linearity in R2-CPMG dispersion are highlighted (cyan). The mutated sites R55 (green) and K82 (red) are also shown. **(C)** H(S/M)QC exchange induced shifts exhibit a similar linear dependence upon mutagenesis as the amplitudes in R2-CPMG profiles. These shifts are colored as in (A). [Color figure can be viewed in the online issue, which is available at [www.interscience.wiley.com](http://www.interscience.wiley.com).]

that the imparted changes are not simply local environmental changes (i.e.,  $\Delta\omega$ ), but rather real changes to the dynamics of this region. However, there are very likely local chemical shift changes induced by these mutations as well and this could potentially be why changes imparted to chemical exchange for each residue do not increase or decrease exactly the same. Alternatively, since we have shown earlier that residues within each region exhibit different exchange

rates this may also imply that the mutations result in somewhat different effects on sampled populations.

A secondary measure of this mutagenic additive effect for CypA is shown using H(S/M)QC experiments [Fig. 4(C)]. This ingenious combination of two routinely used NMR experiments takes advantage of the fact that residues undergoing exchange give rise to small chemical shift differences between an HSQC spectrum and an HMQC spectrum.<sup>27</sup> The same subset of residues exhibiting an additive effect to  $R_{ex}$  as measured through R2-CPMG experiments also exhibit a similar linearity for H(S/M)QC induced shifts (note that the measured value in Hz is actually  $\Omega/2\pi$ ). From Eq. (3) (Materials and Methods), either  $k_A$  or  $k_B$  could theoretically be responsible for the observed changes in these measured  $\Omega/2\pi$  values. However, these mutations do not significantly alter the  $k_{ex}$  values extracted from R2-CPMG fits of each residue that is dominated by  $k_B$  (i.e.  $P_A$ ) and, thus, the amplitude changes must be due to  $k_A$  (i.e.  $P_B$ ). As described earlier, these mutagenic changes to dynamics are not simply due to altered chemical environments (i.e.  $\Delta\omega$ ) since they are found to uniformly either decrease or increase amplitudes within CypA<sup>R55A</sup> and CypA<sup>K82A</sup> for this region, respectively, for both R2-CPMG dispersions and H(S/M)QC induced shifts. Moreover, the use in this study of high field instrumentation has allowed for the detection of changes that are even further away from the individual sites of the mutations than those previously identified.<sup>8</sup> For example, the amide of V29 is nearly 25 Å from the mutated side chain of R55 within CypA<sup>R55A</sup> and a change in  $\Delta\omega$  for V29 (i.e.  $\Delta\omega_N$ ) is not likely the cause for such distal changes in chemical exchange [Fig. 4(A,B)]. Thus, once again we conclude that these mutagenic changes are due to the minor population (i.e.  $P_B$ ) and are therefore primarily thermodynamic in nature.

**Residues in which chemical exchange within CypA<sup>R55A,K82A</sup> is NOT a linear combination of that within CypA<sup>R55A</sup> and CypA<sup>K82A</sup> (regions II and III)**

As opposed to residues within region I that exhibit an additive effect to chemical exchange from both individual mutations within CypA<sup>R55A,K82A</sup>, regions II and III do not. Interestingly, the mutation of K82A alone uniformly increases the contribution to exchange for every single residue throughout the enzyme with detectable R2-CPMG dispersion (i.e. regions I, II, and III), suggesting a global increase of their minor sampled conformations. This in itself is a striking finding, since there is more than 20 Å between the side chain of K82 and some of the residues found to be dynamically affected by its mutation. Interestingly, there is no difference in the chemical denaturation of CypA<sup>K82A</sup> relative to wild-type CypA (data not shown), suggesting such an increase is not simply due to protein instability. In contrast, it is the mutation of R55A



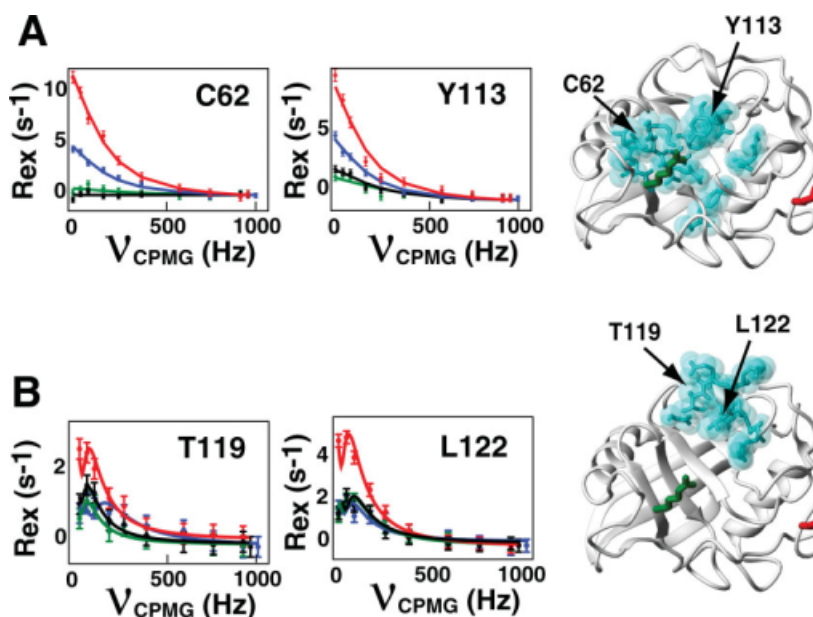


**Figure 5.** The chemical exchange of many residues of CypA is uncoupled through mutagenesis (described as regions II and III). All residues exhibit an increase in their sampling of a minor population upon mutagenesis of K82 (CypA<sup>K82A</sup>, red) relative to the wild type CypA (blue) as shown by the amplitude of R2-CPMG dispersion curves. However, this is not the case for the mutation of R55A. **(A)** For residues within region II, which include C62 and Y113, the mutation of R55A (CypA<sup>R55A</sup>, green) induces a decrease in the sampling of these minor populations and renders the enzyme insensitive to the further mutation of K82A (CypA<sup>R55A,K82A</sup>, black). Residues exhibiting a similar mutagenic dependence are shown (cyan). **(B)** For residues within region III, which include T119 and L122, the mutation of R55A induces a negligible effect on the measured exchange, but also renders the enzyme primarily insensitive to the mutation of K82A. R2-CPMG dispersion profiles are shown for <sup>2</sup>H<sup>15</sup>N-labeled proteins at 0°C. [Color figure can be viewed in the online issue, which is available at [www.interscience.wiley.com](http://www.interscience.wiley.com).]

that results in distinctive differences to each of the three regions. Specifically, the R55A mutation relegates residues within both regions II and III relatively insensitive to the increase in chemical exchange caused by K82A alone. In other words, in region I described above the mutations of R55A and K82A can either decrease or increase the sampling of each residue's minor population, respectively, yet the mutation of R55A appears to decouple much of the remaining dynamic network of CypA that comprise regions II and III described further later.

The defining distinction between regions II and III is their response to the mutation R55A. For example, residues within region II that primarily comprise the active site of CypA ( $\beta$ -strands 3–6) exhibit smaller exchange contributions for CypA<sup>R55A</sup> than the wild-type enzyme [Fig. 5(A)]. In contrast, residues within region III differ from the other regions in that the exchange within CypA<sup>R55A</sup> is essentially the same as the wild-type enzyme [Fig. 5(B)]. Again, the K82A mutation in the context of this CypA<sup>R55A,K82A</sup> has little effect on these regions in sharp contrast to its effect in the context of CypA<sup>K82A</sup>. Thus, if the inherent dynamics of CypA have been evolutionarily conserved to

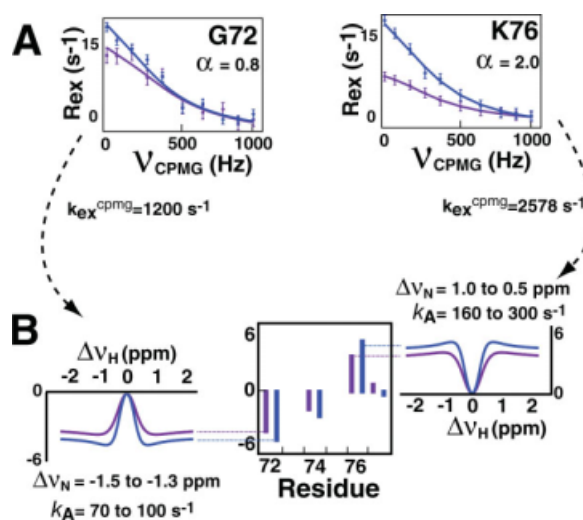


**Figure 6.** Combining R2-CPMG dispersion data with H(S/M)QC exchange induced shifts. **(A)** Chemical exchange rates derived from R2-CPMG data were used with **(B)** H(S/M)QC exchange induced shifts to help define the range in the forward rate constant,  $k_A$ , on a per residue basis. Ranges in  $k_A$  and  $\Delta V_N$  are shown for R<sup>2</sup>-least-squares-fits greater than 0.98 using Eq. (3) as described in Materials and Methods. [Color figure can be viewed in the online issue, which is available at [www.interscience.wiley.com](http://www.interscience.wiley.com).]

maintain its catalytic function, altering the conserved catalytic residue R55 would be expected to disrupt the dynamic network as we have found here.

### The static magnetic field dependence of H(S/M)QC shifts

Although H(S/M)QC shifts were developed to provide the sign of  $\Delta\omega$ ,<sup>27</sup> the field dependence of these shifts also provides useful information. In retrospect, this is not surprising since just as the static magnetic field dependence of chemical exchange (i.e.  $R_{\text{ex}}$ ) provides important insight,<sup>23</sup> so do H(S/M)QC shifts measured at multiple static fields. Specifically,  $k_{\text{ex}}$  is well-determined for most residues from R2-CPMG data alone, but the individual microscopic rate constants that comprise  $k_{\text{ex}}$  are poorly determined (i.e.  $k_A$ ,  $k_B$ ). This is especially true for residues undergoing fast exchange [Eq. (1)], since only  $P_A^*P_B^*\Delta\omega_N$  can be accurately determined and not the individual values (note that  $P_A/P_B = k_B/k_A$ ). However, by combining  $k_{\text{ex}}$  extracted from R2-CPMG dispersion with H(S/M)QC shifts measured at multiple fields, a much narrower range in the microscopic rate constants can be determined. Our discussion will be focused on CypA residues exhibiting both large chemical shifts and undergoing fast exchange on the chemical shift timescale that is localized to several residues within region I. This is because residues exhibiting either small chemical shift differences between sampled states (either  $\Delta\omega_N$  or  $\Delta\omega_H$ ) or undergoing very slow exchange ( $k_{\text{ex}} \ll \Delta\omega_N$ ) do not give rise to measurable H(S/M)QC exchange-induced shifts, as originally described by Skrynnikov *et al.*<sup>27</sup> and shown in Eq. (3). All H(S/M)QC data were collected at 10°C and, thus, have been analyzed jointly using R2-CPMG measurements at the same temperature.

R2-CPMG data were combined with H(S/M)QC data to extract  $\Delta\omega_N$  and  $k_A$  (and thus,  $k_B$ ) on a per residue basis that also provides  $\Delta\omega_H$  as well ( $\Delta v_N$  and  $\Delta v_H$  will be used herein instead of  $\Delta\omega_N$  and  $\Delta\omega_H$ , respectively, since it is simpler to report these extracted values in ppm).  $k_{\text{ex}}$  values derived from R2-CPMG dispersion data were used to calculate H(S/M)QC exchange induced shifts ( $\Omega^{\text{calc}}$ ) using Eq. (3) for a large range in  $\Delta v_H$  values with the experimental H(S/M)QC shifts used as constraints [Fig. 6(A,B)]. Although analogous <sup>1</sup>H-R2-CPMG dispersion data would provide the explicit  $\Delta v_H$  for each residue, this is unnecessary as  $\Omega^{\text{calc}}$  is essentially unchanged beyond  $\Delta v_H$  values of  $\sim|0.25|$  ppm. This is a reasonable assumption for most residues, since large  $\Delta v_N$  are likely associated with large  $\Delta v_H$ . A range in  $k_A$  and  $\Delta v_N$  can adequately describe the experimentally observed shifts at both fields [Fig. 6(B)]. The use of two static magnetic field strengths was important (i.e. 600 and 900 MHz) since matching  $\Omega^{\text{calc}}$  to a single static magnetic field did not offer any advantage over using R2-CPMG data alone. Finally, the static mag-

netic field dependence of  $R_{\text{ex}}$  for these residues (i.e. the  $\alpha$  values) provides additional validation of our calculations and is consistent with the measured ranges in  $\Delta v_N$  values extracted from our fits. For example, K76 undergoes fast exchange ( $\alpha = 2.0$ ) and with  $k_{\text{ex}} \sim 2600 \text{ s}^{-1}$  this means  $\Delta v_N$  must be less than  $\sim 4$  ppm at 900 MHz that is indeed the case for the range calculated [Fig. 6(B), right]. G72 undergoes intermediate exchange ( $\alpha = 1$ ) and with  $k_{\text{ex}} = 1200 \text{ s}^{-1}$  this means  $\Delta v_N$  is approximately 2 ppm at 900 MHz that is close to the range found for the H(S/M)QC fits [Fig. 6(B), left].

A total of five residues could be fit using this analysis that included G65, F67, N71, G72, and K76 with similar extracted  $k_A$  values ranging from 70 to 300  $\text{s}^{-1}$ . While these ranges in both  $k_A$  (i.e.  $P_B$ ) and  $\Delta v_N$  are slightly less than those using R2-CPMG data alone, they are still relatively large. The quantitative reason is analogous to chemical exchange where the product  $P_B^*\Delta v_N$ , in Eq. (1) is similar to the functional form of  $k_A^*\Delta v_N$  in Eq. (3). Moreover, uncertainties in  $\Omega/2\pi$  could potentially be as large as 0.5  $\text{s}^{-1}$  and, therefore, these ranges are likely to be even larger.<sup>27</sup> Additional H(S/M)QC exchange induced shifts measured at more static magnetic field strengths would reduce these uncertainties. Nonetheless, several important semi-quantitative conclusions may be drawn. First, these calculations suggest that the measured exchange is well-described by a two-site model that we have used to calculate  $\Omega^{\text{calc}}$  values<sup>27</sup> and is thus consistent with our measured mutagenic regulation of these residues that also support a dominant two-site exchange model. Second, the extracted ranges in  $k_A$  values for these residues within region I are approximately two orders of magnitude larger than that of residues 119–122 of region III, suggesting that there is a large variation in the microscopic rate constants across the enzyme as expected by their variation in the observed  $k_{\text{ex}}$  for these residues (see Fig. 2).

### Discussion

In this report, we have identified numerous residues within free CypA that undergo exchange and amount to nearly half of the enzyme. The majority of residues exhibiting exchange are relegated to the active site and regions immediately proximal to the active site [Fig. 1(A), Supporting Information Table S2]. This inherent exchange of nearly the entire CypA active site supports our previous proposal that the inherent movements of the enzyme have been evolutionarily selected for its catalytic function.<sup>8</sup> This notion that macromolecular motions, and particularly enzyme motions, have accrued specific inherent properties along with their structural fold is also called “conformational selection” and has previously been proposed.<sup>28</sup> This model predicts that important dynamic transitions occur and could suggest that CypA, for example, undergoes a conformational exchange similar to its *cis/trans*

isomerization even in the absence of substrates. This is further supported by our findings here that have shown that even the catalytic residue R55 exhibits an exchange rate similar to its catalytic rate of turnover of small model peptides.<sup>29</sup> We note that the theory of “conformational selection” is similar to the Monod, Wyman, and Changeux (MWC) model proposed more than 40 years ago<sup>30</sup> and the recent advances in NMR solution methods that probe chemical exchange have provided our first “glimpse” of these dynamic transitions to low-populated conformations.

We have obtained several experimental lines of evidence that indicate the inherent exchange within free CypA represents numerous dynamic events. First, there is a “dynamic continuum” of exchange that varies from  $\sim 1000$  to  $\sim 6000$   $s^{-1}$  in the extracted  $k_{ex}$  values from R2-CPMG dispersions at 20°C and this is even visually apparent in the raw data [Fig. 2(B)]. The differential exchange rates of several residues that are structurally close to one another, such as K82, N102, and S110, suggest that the dominant contributions to exchange are highly localized (i.e. potentially arising from side chain motions). Thus, while it has become commonplace to globally fit R2-CPMG dispersion if residues exhibit similar exchange rates, such a single global process is an oversimplification for free CypA. Moreover, without the preexisting knowledge of residues that may be involved in a single global cooperative event, such as the folding/unfolding of a protein,<sup>5,31</sup> there is no apparent rationale for this within CypA or even an indication as to which residues should be globally fit. Second, forward rate constants (i.e.  $k_A$ ) for each residue also exemplify large differences between different regions of CypA. For example, for residues such as those within the 3,10- $\alpha$ -helix of residues 119–122 and neighboring residues that are at the limit of slow exchange (i.e.  $\alpha = 0$ ),  $k_A$  is in the order of  $R_{ex}$ <sup>3</sup> and is approximately 1–2  $s^{-1}$  [as shown in Fig. 1(B) for L122 and Fig. 3B for T119]. In contrast,  $k_A$  values likely begin at  $\sim 70$   $s^{-1}$  for the faster exchanging residues that reside within residues 65–84 that could be analyzed using both R2-CPMG and H(S/M)QC data (see Fig. 6). Thus, there is two orders of magnitude difference on the timescale of seconds for the forward microscopic rate constants of CypA. Third, residues within CypA exhibit different temperature dependencies (see Fig. 3). For example, many of the core residues of CypA that include residues within the  $\beta$ -sheet at the bottom of the active site exhibit the least temperature dependencies (e.g. F113 in Fig. 3), while most other residues do exhibit significant temperature dependencies (e.g. T119 and I78 in Fig. 3). Finally, despite this data that indicates CypA undergoes multiple exchange processes, we have also shown that these independent processes are at least partially coupled. The K82A mutation illustrates such coupling since this point mutation induces a global increase in the sampling of the minor population for all residues exhibit-

ing measurable exchange. Thus, the dynamic behavior within free CypA includes a complicated array of dynamic events that comprise predominantly independent dynamic processes on the  $\mu s$ -ms timescale that are, nonetheless, at least partially coupled.

Although NMR relaxation experiments have provided dynamic details at atomic resolution that are difficult to obtain through standard structural techniques, there is still a gap in bridging the physical movements of dynamics with the measured exchange. At the heart of understanding this relationship is identifying the number of conformations that chemical exchange monitors. To this end, we have utilized a combination of mutagenesis and NMR relaxation to probe the number of conformations sampled by CypA and we have found that much of the residues exchange between two dominant conformations. Specifically, by combining individual mutations that either decrease or increase a minor sampled population for residues within the enzyme (i.e. CypA<sup>R55A</sup> and CypA<sup>K82A</sup>, respectively), we have produced a double mutant (i.e. CypA<sup>R55A,K82A</sup>) that exhibits near wild-type exchange for much of the enzyme, described as region I (see Fig. 4). This linear combination of the individual mutagenic changes implies that these residues undergo a dominant two-site exchange and also suggests that we have been able to selectively “dial” the dynamics of much of CypA by combining point mutations. Interestingly, several residues within these same residues of 65–84 also make direct contacts with the N-terminal residues of substrates<sup>32,33</sup> and have previously been proposed to be isomerized relative to the substrate peptidyl–prolyl bond.<sup>34</sup> Thus, just as CypA catalyzes substrates between two conformations (i.e. the cis and trans conformations), the inherent movements of at least a large fraction of CypA, described as region I here (see Fig. 4), already undergoes a similar two-state conformational exchange prior to substrate engagement. The fact that this linear effect from each mutation is not observed for the remaining regions of CypA, defined as regions II and III (see Fig. 5), does not necessarily imply that the remaining residues undergo a more complicated process. This is because the R55A mutation appears to simply uncouple much of the motions of the enzyme and render residues within these regions insensitive to the K82A mutation. Such a central role of R55 in coupling the dynamic network of CypA is not surprising in retrospect, since R55 is the catalytically conserved residue and would thus be expected to play an important role in the dynamic network.<sup>35,24,25,14</sup>

In summary, we have shown that CypA undergoes dynamic exchange on both multiple chemical shift timescales (i.e.  $k_{ex}/\Delta\omega$ ) as well as multiple absolute timescales (i.e.  $k_{ex}$ ) and that the exchange of at least part of the enzyme can be specifically controlled (or “dialed”) by mutagenesis. In other words, analogous to a volume control that can either be lowered or

increased, we have used mutagenesis to control the conformational sampling of the enzyme's minor states ( $P_B$ ) for many residues of CypA. Extending this work to studies that include CypA/substrate complexes during turnover will be a powerful way to identify motions that directly correlate to catalysis. For example, the placement of a substrate within the active site may completely couple the different exchange events identified within free CypA. Our previous work employed a model peptide substrate and only detected a few residues that exhibited large chemical exchange differences between the free enzyme and active enzyme/substrate complex.<sup>8</sup> This was likely due to the sensitivity limit of using only  $^{15}\text{N}$ -labeled protein at a single field and a single temperature. Unfortunately, such model peptides bind too weakly to monitor the active complex at the multiple temperatures probed in this study, since it is not possible to fully saturate CypA with such peptides and thereby isolate the catalytic events ( $K_d \sim 1 \text{ mM}$ ).<sup>14</sup> Conversely, the use of larger proteins such as the HIV-CA that binds to CypA with a much higher affinity ( $K_d \sim 15 \mu\text{M}$ ) would be difficult to monitor at the lower temperatures due to the relatively large size of this CypA/HIV-CA complex.<sup>32</sup> However, a recent phage-display study has revealed several potential peptide substrates that bind nearly an order of magnitude tighter than most model peptides studied to date<sup>36</sup> and a current focus within our lab is to identify such a tightly binding substrate to readily study active cyclophilins at multiple temperatures. Nonetheless, the current study has shown that multiple exchange events occur within free CypA and that point mutations can be rationally combined to induce distal dynamic effects throughout large regions of a protein. This may have major implications for the rational design of enzymes with specific dynamic and thereby catalytic properties in the future.

## Materials and Methods

### *Protein expression, purification, and sample preparation*

Wild-type CypA and all mutants were grown in M9 minimal media supplemented with either  $^{15}\text{N}$ -ammonium chloride for  $^{15}\text{N}$ -labeled samples or both  $^{15}\text{N}$ -ammonium chloride and 99%  $\text{D}_2\text{O}$  for  $^2\text{H},^{15}\text{N}$ -labeled samples. Although unlabeled glucose was used for all growths, similar extents of deuteration was shown by the fact that each  $^2\text{H},^{15}\text{N}$ -labeled protein required twice the constant time relaxation period to monitor R2-CPMG dispersion as its  $^{15}\text{N}$ -labeled counterpart (see NMR Spectroscopy and Analysis). All proteins were encoded within the pET3a plasmid and BL21(DE3) cells were used for all cell growths supplemented with ampicillin. Proteins purified from the soluble fractions or refolded from insoluble fractions as previously described<sup>8</sup> produced identical spectra,

and thus, both fractions were combined to maximize yields. All proteins were purified via ion-exchange chromatography using SP- and Q-sepharose as previously described.<sup>14</sup> However, an additional S-100 size exclusion step was also applied. This latter step was originally found necessary for  $^2\text{H},^{15}\text{N}$ -labeled purifications that yielded far less protein, and thus, larger relative impurities, and required up to 4L growths to produce highly concentrated samples. All purifications were conducted on an AKTA FPLC system (GE Healthcare). Final samples for NMR contained 2.0 mM protein in 50 mM  $\text{Na}_2\text{HPO}_4$ , pH 6.5, 2 mM DTT with 5%  $\text{D}_2\text{O}$ .

### *NMR spectroscopy and analysis*

Transverse Relaxation Optimized Spectroscopy (TROSY)-based  $^{15}\text{N}$ -R2-CPMG pulse sequences were applied for relaxation dispersion experiments<sup>37</sup> and HSQC/HMQC pulse sequences were applied to measure exchange-induced shifts<sup>27</sup> on either a Varian 600 or 900 MHz spectrometer collected at 0, 10, or 20°C as indicated. Relaxation compensated pulse sequences for all R2-CPMG experiments were employed.<sup>38,39</sup>

A total of 18  $^{15}\text{N}$ -R2-CPMG experiments were collected using a constant relaxation delay time and varying the applied refocusing field  $\nu_{\text{cpmg}}$ . At least 10 different refocusing fields were collected for each data set and their  $R_2^{\text{eff}}$  calculated as previously described.<sup>40</sup> These data sets include the following:  $^{15}\text{N}$ -R2-CPMG data sets were initially collected at 600 MHz at 10°C on  $^{15}\text{N}$ -labeled wild-type CypA, CypA<sup>R55A</sup>, CypA<sup>K82A</sup>, and CypA<sup>R55A,K82A</sup> (four total thus far). All the four proteins were then  $^2\text{H},^{15}\text{N}$ -labeled to monitor their dispersion at 900 MHz at both 0 and 10°C (12 total thus far). Two data sets of  $^{15}\text{N}$ -labeled wild-type at 900 MHz at both 0 and 10°C were collected to ensure their dispersion matched that of the  $^2\text{H},^{15}\text{N}$ -labeled counterpart at the same temperatures (14 total thus far). Finally,  $^{15}\text{N}$ -R2-CPMG data sets were collected on  $^2\text{H},^{15}\text{N}$ -labeled wild-type CypA at 600 MHz at 0, 10, and 20°C and at 900 MHz at 20°C so that the static magnetic field dependence could be compared at all three temperatures studied (18 total). Constant time relaxation periods (i.e. T2 relaxation delays) were optimized for approximately half the intensity of the normalization spectra, which for  $^{15}\text{N}$ -labeled proteins was 20 and 30 ms at 0 and 10°C, respectively, and for  $^2\text{H},^{15}\text{N}$ -labeled proteins was 50, 60, and 80 ms at 0, 10, and 20°C, respectively. Spectra were processed and peak heights extracted using in-house scripts with NMRPipe software.<sup>41</sup> Dispersion analysis was initially conducted using the least squares fitting program CPMG\_FIT, kindly provided by Dr. Dmitry Korzhnev (Departments of Molecular & Medical Genetics & Biochemistry, University of Toronto, Ontario, Canada). CPMG\_FIT employs the generalized two-site Carver-Richards equations that can be applied to up to a three-site exchange<sup>20</sup> and uncertainties for the fit

exchange rates (i.e.  $k_{\text{ex}}$ ) are reported for  $P$ -values less than 0.05. For residues undergoing fast exchange (i.e.  $k_{\text{ex}} \gg 1000 \text{ s}^{-1}$ ) application of the Luz-Meiboom approximation<sup>42</sup> using Prism 4.0 (GraphPad Software) was found to result in similar exchange rates (data not shown). Residues undergoing slow exchange at 0 and 10°C, as identified by their static magnetic field dependence, were further analyzed using Prism 4.0 with Eq. (2).<sup>3</sup>

A total of 13 H(S/M)QC experiments were collected. These included <sup>15</sup>N-labeled wild-type CypA, CypA<sup>R55A</sup>, CypA<sup>K82A</sup>, and CypA<sup>R55A,K82A</sup> at 600 MHz at 10°C and their <sup>2</sup>H,<sup>15</sup>N-labeled counterparts at 900 MHz at both 0 and 10°C. An additional data set of <sup>2</sup>H,<sup>15</sup>N-labeled wild-type CypA was also collected at 600 MHz and 10°C to compare with the same wild-type CypA at 900 MHz at the same static field. H(S/M)QC exchange induced shifts were calculated using CCPNmr software.<sup>43</sup> Theoretical H(S/M)QC exchange induced shifts were calculated using  $k_{\text{ex}}$  ( $= k_A + k_B$ ) extracted from the residue specific <sup>15</sup>N-R2-CPMG dispersion using Prism 4.0 with the following equation as previously described.<sup>27</sup>

$$\Omega_N = k_a \left[ \frac{\Delta\omega_N/k_b}{1 + (\Delta\omega_N/k_b)^2} \right] - \frac{k_a}{2} \left[ \frac{\Delta\omega_N/k_b + \Delta\omega_H/k_b}{1 + (\Delta\omega_N/k_b + \Delta\omega_H/k_b)^2} \right] - \frac{k_a}{2} \left[ \frac{\Delta\omega_N/k_b - \Delta\omega_H/k_b}{1 + (\Delta\omega_N/k_b - \Delta\omega_H/k_b)^2} \right] \quad (3)$$

## Acknowledgments

This work was supported by the National Science Foundation (grant #MC8Bo820567). All NMR experiments collected at 600 MHz were conducted at the National High Magnetic Field Laboratory (NHMFL) supported by cooperative agreement DMR 0654118 between the National Science Foundation and the State of Florida. All NMR experiments collected at 900 MHz were conducted at the Rocky Mountain 900 Facility (grant #NIHGM68928). The authors thank Dr. Dmitry Korzhnev, Departments of Molecular & Medical Genetics & Biochemistry, University of Toronto, Ontario, Canada, for the program CPMG\_FIT and many helpful discussions.

## References

1. Grey MJ, Wang CY, Palmer AG (2003) Disulfide bond isomerization in basic pancreatic trypsin inhibitor: multi-site chemical exchange quantified by CPMG relaxation dispersion and chemical shift modeling. *J Am Chem Soc* 125: 14324–14335.
2. Hill RB, Bracken C, DeGrado WF, Palmer AG (2000) Molecular motions and protein folding: characterization of the backbone dynamics and folding equilibrium of alpha D-2 using C-13 NMR spin relaxation. *J Am Chem Soc* 122: 11610–11619.
3. Tollinger M, Skrynnikov NR, Mulder FAA, Forman-Kay JD, Kay LE (2001) Slow dynamics in folded and unfolded states of an SH3 domain. *J Am Chem Soc* 123: 11341–11352.
4. Korzhnev DM, Karlsson BG, Orekhov VY, Billeter M (2003) NMR detection of multiple transitions to low-populated states in azurin. *Protein Sci* 12: 56–65.
5. Korzhnev DM, Neudecker P, Zarrine-Afsar A, Davidson AR, Kay LE (2006b) Abp1p and fyn SH3 domains fold through similar low-populated intermediate states. *Biochemistry* 45: 10175–10183.
6. Lundstrom P, Akke M (2005) Off-resonance rotating-frame amide proton spin relaxation experiments measuring microsecond chemical exchange in proteins. *J Biomol NMR* 32: 163–173.
7. Belshaw PJ, Meyer SD, Johnson DD, Romo D, Ikeda Y, Andrus M, Alberg DG, Schultz LW, Clardy J, Schreiber SL (1994) Synthesis, structure and mechanism in immunophilin research. *Synlett* 381–392.
8. Eisenmesser EZ, Millet O, Labeikovsky W, Korzhnev DM, Wolf-Watz M, Bosco DA, Skalicky JJ, Kay LE, Kern D (2005) Intrinsic dynamics of an enzyme underlies catalysis. *Nature* 438: 117–121.
9. Boehr DD, McElheny D, Dyson HJ, Wright PE (2006b) The dynamic energy landscape of dihydrofolate reductase catalysis. *Science* 313: 1638–1642.
10. Boehr DD, Dyson HJ, Wright PE (2006a) An NMR perspective on enzyme dynamics. *Chem Rev* 106: 3055–3079.
11. Cole R, Loria JP (2002) Evidence for flexibility in the function of ribonuclease A. *Biochemistry* 41: 6072–6081.
12. Beach H, Cole R, Gill ML, Loria JP (2005) Conservation of mu s-ms enzyme motions in the apo- and substrate-mimicked state. *J Am Chem Soc* 127: 9167–9176.
13. Kovrigin EL, Loria JP (2006) Enzyme dynamics along the reaction coordinate: the critical role of a conserved residue. *Biochemistry* 45: 2636–2647.
14. Eisenmesser EZ, Bosco DA, Akke M, Kern D (2002) Enzyme dynamics during catalysis. *Science* 295: 1520–1523.
15. Andreotti AH (2003) Native state proline isomerization: an intrinsic molecular switch. *Biochemistry* 42: 9515–9524.
16. Yao QZ, Li M, Yang H, Chai H, Fisher W, Chen CY (2005) Roles of cyclophilins in cancers and other organ systems. *World J Surg* 29: 276–280.
17. Yurchenko V, Constant S, Bukrinsky M (2006) Dealing with the family: CD147 interactions with cyclophilins. *Immunology* 117: 301–309.
18. Guichou JF, Viaud J, Mettling C, Subra G, Lin YL, Chavanieu A (2006) Structure-based design, synthesis, and biological evaluation of novel inhibitors of human cyclophilin A. *J Med Chem* 49: 900–910.
19. Chen SA, Zhao XM, Tan JZ, Lu H, Qi Z, Huang Q, Zeng XZ, Zhang MJ, Jiang SB, Jiang HL, Yu L (2007) Structure-based identification of small molecule compounds targeting cell cyclophilin A with anti-HIV-1 activity. *Eur J Pharmacol* 565: 54–59.
20. Carver JP, Richards RE (1972) A General two-site solution for the chemical exchange produced dependence of T2 upon the Carr–Purcell pulse separation. *J Magn Reson* 6: 89–105.
21. Jen J (1978) Chemical exchange and NMR T2 Relaxation—multisite case. *J Magn Reson* 30: 111–128.
22. Davis DG, Perlman ME, London RE (1994) Direct measurements of the dissociation-rate constant for inhibitor-enzyme complexes via the T-1-Rho and T-2 (Cpmg) methods. *J Magn Reson Ser B* 104: 266–275.
23. Millet O, Loria JP, Kroenke CD, Pons M, Palmer AG (2000) The static magnetic field dependence of chemical

- exchange linebroadening defines the NMR chemical shift time scale. *J Am Chem Soc* 122: 2867–2877.
24. Zhao Y, Ke H (1996a) Crystal structure implies that cyclophilin predominantly catalyzes the trans to cis isomerization. *Biochemistry* 35: 7356–7361.
  25. Zhao YD, Ke HM (1996b) Mechanistic implication of crystal structures of the cyclophilin-dipeptide complexes. *Biochemistry* 35: 7362–7368.
  26. Kovrigin EL, Kempf JG, Grey MJ, Loria JP (2006) Faithful estimation of dynamics parameters from CPMG relaxation dispersion measurements. *J Magn Reson* 180: 93–104.
  27. Skrynnikov NR, Dahlquist FW, Kay LE (2002) Reconstructing NMR spectra of “invisible” excited protein states using HSQC and HMQC experiments. *J Am Chem Soc* 124: 12352–12360.
  28. Berger C, Weber-Bornhauser S, Eggenberger J, Hanes J, Pluckthun A, Bosshard HR (1999) Antigen recognition by conformational selection. *FEBS Lett* 450: 149–153.
  29. Kern D, Kern G, Scherer G, Fischer G, Drakenberg T (1995) Kinetic analysis of cyclophilin-catalyzed prolyl cis/trans isomerization by dynamic NMR spectroscopy. *Biochemistry* 34: 13594–13602.
  30. Monod J, Wynam J, Changeux J-P (1965). On the nature of allosteric transitions: a plausible model. *J Mol Biol* 12: 88–118.
  31. Korzhnev DM, Bezsonova I, Evanics F, Taulier N, Zhou Z, Bai YW, Chalikian TV, Prosser RS, Kay LE (2006a) Probing the transition state ensemble of a protein folding reaction by pressure-dependent NMR relaxation dispersion. *J Am Chem Soc* 128: 5262–5269.
  32. Gamble TR, Vajdos FF, Yoo SH, Worthylake DK, Houseweart M, Sundquist WI, Hill CP (1996) Crystal structure of human cyclophilin A bound to the amino-terminal domain of HIV-1 capsid. *Cell* 87: 1285–1294.
  33. Ke HM, Huai Q (2004) Crystal structures of cyclophilin and its partners. *Front Biosci* 9: 2285–2296.
  34. Howard BR, Vajdos FF, Li S, Sundquist WI, Hill CP (2003) Structural insights into the catalytic mechanism of cyclophilin A. *Nat Struct Biol* 10: 475–481.
  35. Zydowsky LD, Etkorn FA, Chang HY, Ferguson SB, Stolz LA, Ho SI, Walsh CT (1992) Active site mutants of human cyclophilin A separate peptidyl-prolyl isomerase activity from cyclosporin A binding and calcineurin inhibition. *Protein Sci* 1: 1092–1099.
  36. Piotukh K, Gu W, Kofler M, Labudde D, Helms V, Freund C (2005) Cyclophilin a binds to linear peptide motifs containing a consensus that is present in many human proteins. *J Biol Chem* 280: 23668–23674.
  37. Loria JP, Rance M, Palmer AG (1999b) A TROSY CPMG sequence for characterizing chemical exchange in large proteins. *J Biomol NMR* 15: 151–155.
  38. Loria JP, Rance M, Palmer AG (1999a) A relaxation-compensated Carr-Purcell-Meiboom-Gill sequence for characterizing chemical exchange by NMR spectroscopy. *J Am Chem Soc* 121: 2331–2332.
  39. Wang CY, Palmer AG (2003) Solution NMR methods for quantitative identification of chemical exchange in N-15-labeled proteins. *Magn Reson Chem* 41: 866–876.
  40. Mulder FAA, Skrynnikov NR, Hon B, Dahlquist FW, Kay LE (2001) Measurement of slow ( $\mu$ s-ms) time scale dynamics in protein side chains by N-15 relaxation dispersion NMR spectroscopy: Application to Asn and Gln residues in a cavity mutant of T4 lysozyme. *J Am Chem Soc* 123: 967–975.
  41. Delaglio F, Grzesiek S, Vuister GW, Zhu G, Pfeifer J, Bax A (1995) NMRPipe - a multidimensional spectral processing system based on UNIX pipes. *J Biomol NMR* 6: 277–293.
  42. Luz Z, Meiboom S (1963) Nuclear magnetic resonance study of the protolysis of trimethylammonium ion in aqueous solution-order of the reaction with respect to solvent. *J Chem Phys* 39: 366–370.
  43. Vranken WF, Boucher W, Stevens TJ, Fogh RH, Pajon A, Llinas P, Ulrich EL, Markley JL, Ionides J, Laue ED (2005) The CCPN data model for NMR spectroscopy: development of a software pipeline. *Proteins-Structure Function and Bioinformatics* 59: 687–696.